

Universal non-Hermitian transport in disordered systems

Bo Li,^{1,2} Chuan Chen,^{3,2} and Zhong Wang^{2,*}

¹MOE Key Laboratory for Nonequilibrium Synthesis and Modulation of Condensed Matter, Shaanxi Province Key Laboratory of Quantum Information and Quantum Optoelectronic Devices, School of Physics, Xi'an Jiaotong University, Xi'an 710049, China

²Institute for Advanced Study, Tsinghua University, Beijing, 100084, China

³Lanzhou Center for Theoretical Physics, Key Laboratory of Quantum Theory and Applications of MoE, Key Laboratory of Theoretical Physics of Gansu Province, and School of Physical Science and Technology, Lanzhou University, Lanzhou, Gansu 730000, China

In disordered Hermitian systems, localization of energy eigenstates prohibits wave propagation. In non-Hermitian systems, however, wave propagation is possible even when the eigenstates of Hamiltonian are exponentially localized by disorders. We find in this regime that non-Hermitian wave propagation exhibits novel universal scaling behaviors without Hermitian counterpart. Furthermore, our theory demonstrates how the tail of imaginary-part density of states dictates wave propagation in the long-time limit. Specifically, for the three typical classes, namely the Gaussian, the uniform, and the linear imaginary-part density of states, we obtain logarithmically suppressed sub-ballistic transport, and two types of subdiffusion with exponents that depend only on spatial dimensions, respectively. Our work highlights the fundamental differences between Hermitian and non-Hermitian Anderson localization, and uncovers unique universality in non-Hermitian wave propagation.

The Anderson localization is one of the most prominent phenomena in random systems [1]. It has twofold meanings. The spectral meaning is the localization of eigenstates, while the dynamic meaning is the absence of diffusion. It is generally perceived that the spectral localization always implies dynamical localization. For example, when the electron eigenstates at the Fermi level are Anderson-localized, electron transport is prohibited in a crystal, resulting insulating behavior at low temperature. In sharp contrast to this scenario, recent experiments in open or non-Hermitian systems have found that, despite complete localization of eigenstates, wave propagation remains possible [2, 3] (see also related works Refs. [4–9]). In these systems, random gain and loss localize all the eigenstates, yet waves can propagate in a jumpy manner, dynamically evading the localization.

Experimental and numerical findings suggest that this unconventional non-Hermitian transport dramatically differs from typical ballistic or diffusive motions in terms of the relationship between spreading distance and time scale [2]. It is also recognized that the complexity of eigen-energies is essential, indicating the intrinsically non-Hermitian nature of the phenomenon. However, it remains elusive whether the observed unusual dynamics obeys universal laws. Here, we present a quantitative theory that yields universal transport dynamics, which not only explains the previous experimental findings but also predicts new scaling behaviors. Our theory provides an efficient scheme for calculating the universal behaviors from the basic data of the system. Our approach bears some similarity to Mott's variable-range hopping, though the mechanism is quite different [10]. Roughly speaking, the time plays the role of inverse temperature in Mott's picture.

Universal dynamical scaling. To be concrete, we con-

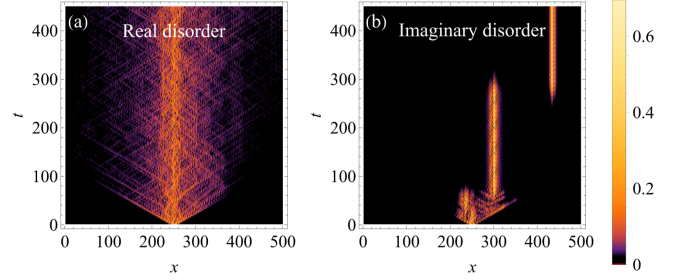


FIG. 1. The space-time evolution of a wave packet initially localized at the center of a chain is plotted under (a) real and (b) imaginary disorder, as described by Eq. (1) (For the real disorder scenario, the imaginary unit in front of the potential is omitted). Here, the disorder respects a uniform distribution $V_x \in [-W, W]$, and $t_0 = 2W = 1$ is used in the plots.

sider a particle moving in a purely imaginary disorder potential

$$H = \sum_{\langle \mathbf{x}, \mathbf{x}' \rangle} t_0 |\mathbf{x}\rangle \langle \mathbf{x}'| + h.c. + i \sum_{\mathbf{x}} V_{\mathbf{x}} |\mathbf{x}\rangle \langle \mathbf{x}| \quad (1)$$

where $\langle \mathbf{x}, \mathbf{x}' \rangle$ stands for the nearest sites on a square-lattice model, t_0 is real, and $V_{\mathbf{x}}$ is a real site-dependent random variable. This model naturally arises in various contexts; for example, it describes classical wave propagation in a lattice with random gain and loss [2] and the dynamics of quantum particles in stochastic dissipative environments (see below). Note that our main results remain applicable if the random potential takes generic complex values, though we shall focus on the simplest cases with purely imaginary values.

Similar to the standard Anderson model, the eigenstates of this Hamiltonian exhibit exponential localization [2, 11]. However, the eigenvalues now take random

complex values. We label the eigenvalues $E_{\mathbf{x}} (\in \mathbb{C})$ and right eigenstates $|\psi_{\mathbf{x}}^R\rangle$ by the localization center \mathbf{x} . Suppose that a particle or wave packet is initially located at $\mathbf{x} = \mathbf{0}$. Its time evolution can be conveniently analyzed in the eigenbasis, i.e., $|\phi(t)\rangle = \sum_{\mathbf{x}} a_{\mathbf{x}}(t) |\psi_{\mathbf{x}}^R\rangle$, where the coefficient has modulus $|a_{\mathbf{x}}(t)| \sim e^{-|\mathbf{x}|/\xi + \lambda_{\mathbf{x}} t}$, ξ being the eigenstate localization length and $\lambda_{\mathbf{x}} = \text{Im}(E_{\mathbf{x}})$. The wave intensity (or particle density) at a position \mathbf{x} at time t is $P(\mathbf{x}, t) \sim e^{2W(\mathbf{x}, t)}$, where $W(\mathbf{x}, t) = -|\mathbf{x}|/\xi + \lambda_{\mathbf{x}} t$ is a weight factor. At each moment, the average position $\mathbf{x}_c = \sum_{\mathbf{x}} \mathbf{x} P(\mathbf{x}, t) / \sum_{\mathbf{x}} P(\mathbf{x}, t)$ is dominated by the localization center of the eigenstate with maximum weight factor, and contribution from other eigenstates are exponentially suppressed. The weight factor measures the competition between the exponential tail suppression ($-|\mathbf{x}|/\xi$) and the temporal amplification ($\lambda_{\mathbf{x}} t$). As time grows, the most probable localization center moves to further positions, spreading the wavepacket over space. Therefore, the average displacement is obtained by optimizing the weight factor at each moment [10, 12–18].

To implement this optimization, we estimate the largest growing factor $\lambda_{|\mathbf{x}|}^{\max}$ within a volume $\sim |\mathbf{x}|^d$. Since $\lambda_{\mathbf{x}}$ follows the same distribution across each site, $W(\mathbf{x}, t)$ is predominantly optimized by $\lambda_{|\mathbf{x}|}^{\max}$ within this volume. This is particularly relevant given the broad distribution of $\lambda_{\mathbf{x}}$ under strong randomness, leading to exponential suppression of other contributions. The probability of selecting a value greater than $\lambda_{|\mathbf{x}|}^{\max}$ is $P_x = \int_{\lambda_{|\mathbf{x}|}^{\max}}^{\infty} d\lambda \rho(\lambda)$, where $\rho(\lambda)$ is the imaginary-spectrum density of state (iDOS). In the considered region, there has to be at least one site taking the value $\lambda_{|\mathbf{x}|}^{\max}$, implying $P_x |\mathbf{x}|^d \sim 1$. This yields [19]:

$$P_x \sim |\mathbf{x}|^{-d}, \quad (2)$$

meaning that P_x should diminish as $|\mathbf{x}|$ grows. This indicates that the long-time scaling behavior is dictated by the tail of iDOS. If the iDOS $\rho(\lambda)$ is specified, the relation between $\lambda_{|\mathbf{x}|}^{\max}$ and $|\mathbf{x}|$ can be further identified with the help of Eq. (2). For instance, if the iDOS respects the Gaussian distribution $\rho(\lambda) \propto e^{-\lambda^2/(2\sigma^2)}$ with σ being the standard deviation, by using the error-function expansion we can obtain $\lambda_{|\mathbf{x}|}^{\max} \sim (d \ln |\mathbf{x}|)^{1/2}$ [20]. Substituting this relation into the weight factor and letting $\frac{dW}{d|\mathbf{x}|} = -\frac{1}{\xi} + \frac{d\lambda_{|\mathbf{x}|}^{\max}}{d|\mathbf{x}|} t = 0$, we arrive at the space-time scaling of location center [20]

$$|\mathbf{x}_c| \sim \frac{t}{(\ln t)^{1/2}}, \quad (3)$$

which implies a sub-ballistic motion. For other distributions, the resulting scaling behaviors are summarized in Table I. Note that the scaling is determined by an integral of iDOS with $\lambda_{|\mathbf{x}|}^{\max}$ being the lower bound. As $\lambda_{|\mathbf{x}|}^{\max}$ increases with spatial distance and time, the effect

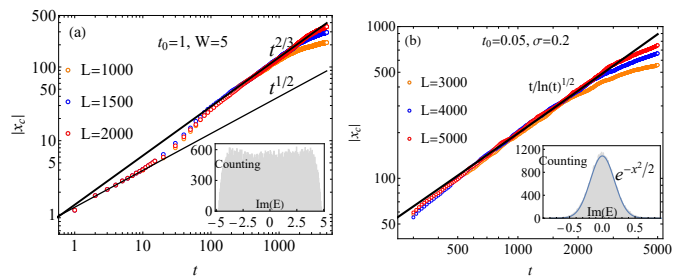


FIG. 2. Dynamical scaling in 1D lattice models with imaginary disorder. (a) For the uniform disorder, where $t_0 = 1$ and $W = 5$, simulations are conducted with 500 realizations of disorder. (b) Gaussian disorder with $t_0 = 0.05$ and $\sigma = 0.2$ is considered, with 1500 realizations of disorder. The data for $\text{Im}(E)$ in both insets are collected from a system with $L = 500$ and 200 trials of disorder.

of iDOS will gradually fade away, leaving its small tail to become predominant in the late-stage dynamics. In this process, crossover from one scaling to another may arise if the iDOS does not respect a universal functional form [e.g., the example in Fig. 2 (a) discussed later].

iDOS	$\rho(\lambda)$	Dyanmical scaling
Gaussian	$e^{-\lambda^2/(2\sigma^2)}$	$ \mathbf{x}_c \sim t / \ln^{1/2} t$
Uniform	const.	$ \mathbf{x}_c \sim t^{1/(d+1)}$
Linear	$a - b\lambda$	$ \mathbf{x}_c \sim t^{2/(d+2)}$

TABLE I. Dynamical scaling for different iDOS. For the linear iDOS, a, b are real parameters. The domain of λ is given to ensure the normalization, not specified here.

1D examples with strong disorder. To validate our dynamic scaling predictions, we conducted numerical simulations for 1D cases, averaging over various disorder realizations [denoted by (\dots)]. The location center distance $|\mathbf{x}_c|$ is calculated numerically by the expected value of spreading distance $\langle |\mathbf{x}| \rangle = \sum_{\mathbf{x}} |\mathbf{x}| \langle |\phi(t)|^2 \rangle / \langle |\phi(t)|^2 \rangle$. In our initial exploration, we examined a uniform disorder potential with $V_x \in [-W, W]$. For sufficiently strong disorder, $W \gg t_0$, dominating the imaginary part of spectrum, the iDOS approximates a uniform distribution $[\rho(\lambda) = \text{const.}]$ except for the linearly decreasing tail $[\rho(\lambda) \sim a - b\lambda]$ near the edge, as depicted in the inset of Fig. 2 (a). As a result, a $|\mathbf{x}_c| \sim t^{1/(d+1)}|_{d=1} = t^{1/2}$ scaling appears in the early stage because P_x in Eq. (2) is mainly dictated by a uniform iDOS; while the late-stage scaling switches to $|\mathbf{x}_c| \sim t^{2/(d+2)}|_{d=1} = t^{2/3}$ as a consequence of the linear tail of iDOS. This prediction aligns well with numerical simulations in Fig. 2 (a), where size-effect-free scaling is evident from the overlap between the curves for different system sizes. The deviation from the thermodynamic-limit trajectory is observed to be delayed for larger systems compared to smaller ones. Here, the linear iDOS tail can be understood by the rare events of

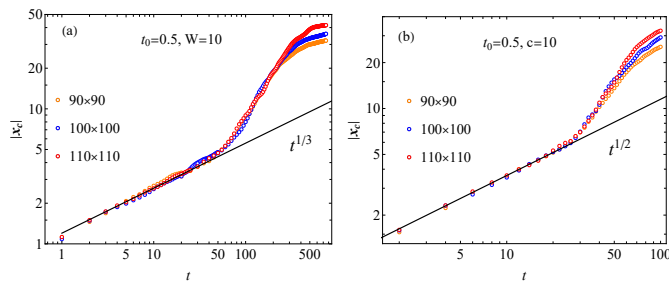


FIG. 3. Dynamical scaling for 2D square-lattice models with system size given by the plot legends, where 500 realizations of disorder are performed. (a) A uniform disorder $V_{\mathbf{x}} \in [-W, W]$ is considered. (b) The disorder respects a right triangle distribution, where c is the length of the base line, see the text.

neighboring sites occupied by potentials with similar values [20]. Moreover, our theory and simulation are fully consistent with the optical experiment [2]. Another significant case involves Gaussian-type iDOS, generated by strong Gaussian imaginary disorder with $\sigma \gg t_0$. As shown in Fig. 2 (b), the numerical data for the larger-size system overlay on top of the smaller one until size effect entering the dynamics. The theoretical prediction in Eq. (3) matches perfectly with the overlapped part at a large time, owing to that Eq. (3) is justified for large λ .

Numerical results for 2D. In Table I, the uniform or linear iDOS result in a dimension-dependent scaling, providing a key feature for verifying our predictions. Similar to the 1D case, a strong uniform disorder in higher dimension is expected to give a iDOS with a linear tail attached to a uniform bulk part. In Fig. 3 (a), we performed simulation for the 2D case, where $|\mathbf{x}_c| \sim t^{1/(d+1)}|_{d=2} = t^{1/3}$ is indeed observed in the early dynamical stage. However, constraints on simulation size prevent observation of late-stage dynamics influenced by the linear iDOS tail. To address dimension sensitivity stemming from a linear iDOS, simulations are conducted under the influence of strong imaginary disorder adhering to a (right angled) triangular distribution, i.e., the probability density follows $f(V_{\mathbf{x}}) = 2(1 - V_{\mathbf{x}}/c)/c$ with $V_{\mathbf{x}} \in [0, c]$ and $t_0 \ll c$. Notably, the predominant linear iDOS profile facilitates rapid manifestation prior to the onset of size effects, thus leveraging the limited size in 2D simulations effectively. In Fig. 3 (b), the expected scaling $|\mathbf{x}_c| \sim t^{2/(d+2)}|_{d=2} = t^{1/2}$ is evident during the early stage, while long-term dynamics are influenced by both size effects and the iDOS tail, which is not of interest here.

Varying disorder strength. In the aforementioned examples, the iDOS predominantly reflects the disorder statistics due to its pronounced influence. Nevertheless, rich forms of iDOS will appear upon decreasing the disorder strength, leading to more intricate scaling behaviors. A scaling crossover is anticipated as disorder strength

varies from strong to weak. For an extremely weak disorder, the scaling approaches to the ballistic transport, where $|\mathbf{x}| \sim t$. This is particularly evident when the system size L is significantly smaller than the localization length ξ so that the wave packet behaves like an extended wave, signifying a size effect. In the thermodynamic limit $L \rightarrow \infty$, the analysis outlined before remains valid, with ξ serving as a new unit length, i.e., the wave packet is still strongly localized in the rescaled system. Despite the coarse-grained unit cell is occupied by many eigenstates, the long-time ($t \gg 1$) probability of the wave packet locating at the new cell positioning at \mathbf{X} is mostly governed by the maximum growing factor $\lambda_{\mathbf{X}}$ therein, represented as $P(\mathbf{X}, t) \sim e^{-|\mathbf{X}|/\xi + \lambda_{\mathbf{X}}t}$, where $\lambda_{\mathbf{X}}$ follows the same distribution as the original $\lambda_{\mathbf{x}}$. Moreover, for sufficiently weak disorder, i.e., $\xi \gg 1$, the central limit theorem requires the original growing factor $\lambda_{\mathbf{x}}$ to respect the Gaussian distribution [20], effectively approximated as an average of $V_{\mathbf{x}}$ within the volume of size ξ^d . Hence, the scaling Eq. (3) is expected for weak disorder in the thermodynamic limit. However, its numerical validation necessitates exceptionally large system sizes, which will be left for future study.

The emerged Gaussian distribution is contingent upon condition $\xi \gg 1$, which gradually breaks down as disorder strength increases until the system approaches the regime of strong disorder, i.e. $\xi \lesssim 1$. In the case of intermediate disorder characterized by $W, \sigma \sim t_0$, the iDOS cannot be easily identified. Consequently, the associated scaling behavior undergoes an unknown crossover bridging the two extreme cases [20].

Renormalization group analysis. From results above, the scaling behavior exhibits high sensitivity to disorder strength. In the regime of weak disorders, our approach necessitates a rescaled interpretation. In this respect, it is helpful to take a view of our problem from renormalization group perspective. In long-wavelength limit, the Hamiltonian Eq. (1) is represented as a Schrödinger equation $i\partial_t\psi(\mathbf{x}, t) = [-D\nabla^2 + iV(\mathbf{x})]\psi(\mathbf{x}, t)$, where the potential respects $\langle V(\mathbf{x})V(\mathbf{x}') \rangle = v\delta^d(\mathbf{x} - \mathbf{x}')$ with $v > 0$ representing the disorder strength. Performing the transformation $\psi(\mathbf{x}, t) = \exp(\Phi(\mathbf{x}, t))$, the Schrödinger equation is converted to a nonlinear equation

$$\partial_t\Phi = iD\nabla^2\Phi + i\eta(\nabla\Phi)^2 + V(\mathbf{x}), \quad (4)$$

where $D = \eta = t_0$. This form allows us to implement a dynamical renormalization group analysis [21, 22]. Following the standard procedure [23], we obtain a flow equation [20]

$$\frac{dg}{dl} = g\left[4 - d + \frac{2(12 - 5d)}{d}K_d g\right], \quad (5)$$

where $g = v\eta^2/D^4$, $K_d = S_d/(2\pi)^d$ with S_d being the solid angle in d dimension, and the rescaling $\mathbf{x} \rightarrow e^l\mathbf{x}$ is performed. The flow equation yields two fixed points,

$g_1^* = 0$, $g_2^* = d(d-4)/[2(12-5d)K_d]$. Notably, g_1^* is unstable for $d < 4$, while g_2^* is physically untenable for $d < 12/5$ due to its negative value, conflicting with the definition. Thus, in 1D and 2D, the system does not transition to new phases upon rescaling, validating our analysis for weak disorders. However, for $d = 3$, $g_2^* = 1/(2K_d)$ is a genuine fixed point. This presents a distinct scenario from real disorder cases, where the leading-order fixed point can be disrupted by higher-order fluctuations [24]. In future, it would be interesting to explore this new phase appearing in 3D.

Liouvillian dynamics. Although the preceding analysis focuses on systems with non-Hermitian Hamiltonians, it is noteworthy that analogous dynamics can arise within the framework of the Liouvillian superoperator. We consider an open system described by the following Lindblad master equation of density matrix $\hat{\rho}$

$$\frac{d\hat{\rho}}{dt} = -i[\hat{H}_0, \hat{\rho}] + \sum_{\mathbf{x}} \gamma_{\mathbf{x}} \mathcal{D}[\hat{a}_{\mathbf{x}}] \hat{\rho} \quad (6)$$

where $\hat{H}_0 = \sum_{\mathbf{x}, \mathbf{x}'} h_{\mathbf{x}, \mathbf{x}'} \hat{a}_{\mathbf{x}}^\dagger \hat{a}_{\mathbf{x}'}$ is a Hermitian Hamiltonian, with $\hat{a}_{\mathbf{x}}^\dagger$ ($\hat{a}_{\mathbf{x}}$) being the creation (annihilation) operator at lattice site \mathbf{x} , and $\mathcal{D}[\hat{a}_{\mathbf{x}}] \hat{\rho} = \hat{a}_{\mathbf{x}} \hat{\rho} \hat{a}_{\mathbf{x}}^\dagger - \frac{1}{2}(\hat{a}_{\mathbf{x}}^\dagger \hat{a}_{\mathbf{x}} \hat{\rho} + \hat{\rho} \hat{a}_{\mathbf{x}} \hat{a}_{\mathbf{x}}^\dagger)$. On the right hand side of Eq. (6), the first term describes an unitary evolution given by \hat{H}_0 , and the second term accounts local losses with site-dependent random rate $\gamma_{\mathbf{x}}$. Using Eq. (6), we can show that two-point correlation function $G_{\mathbf{x}_1, \mathbf{x}_2} = \text{Tr}[\hat{\rho} \hat{a}_{\mathbf{x}_1}^\dagger \hat{a}_{\mathbf{x}_2}]$ satisfies the following matrix equation [20]

$$\frac{dG}{dt} = i(HG - GH^\dagger) \quad (7)$$

where $G = \sum_{\mathbf{x}, \mathbf{x}'} G_{\mathbf{x}, \mathbf{x}'} |\mathbf{x}\rangle \langle \mathbf{x}'|$, and $H = h^T + iV$ describes a Hermitian system h^T subject to a random imaginary disorder iV with $V_{\mathbf{x}, \mathbf{x}'} = \gamma_{\mathbf{x}} \delta_{\mathbf{x}, \mathbf{x}'}$. The equation is solved by $G(t) = e^{iHt} G(0) e^{-iH^\dagger t}$. Considering N bosonic particles (e.g., photons in cavity) initially locate at $\mathbf{x} = \mathbf{0}$, i.e., $G_{\mathbf{x}, \mathbf{x}'}(0) = N \delta_{\mathbf{x}, \mathbf{x}'} \delta_{\mathbf{x}, \mathbf{0}}$, the correlation matrix at time t evolves to $G(t) = N |\phi(t)\rangle \langle \phi(t)|$ where $|\phi(t)\rangle = e^{iHt} |\mathbf{0}\rangle$ acts as a ‘‘quantum state’’ dictated by the ‘‘Hamiltonian’’ H . The probability distribution of surviving particles is given by $P(\mathbf{x}, t) = G_{\mathbf{x}, \mathbf{x}}(t) / \sum_{\mathbf{x}} G_{\mathbf{x}, \mathbf{x}}(t) = |\langle \mathbf{x} | \phi(t) \rangle|^2 / \langle \phi(t) | \phi(t) \rangle$. This coincides exactly with the particle evolution before, indicating the same dynamical scaling behavior in such an open system. Furthermore, similar dynamic behaviors can emerge from purely dissipative systems ($\hat{H}_0 = 0$) by considering suitable dissipators involving adjacent sites [3, 20].

Conclusion. In systems featuring complex disorders, the non-unitary time evolution facilitates a particle’s jumpy motion even amidst eigenstate localization, in sharp contrast to the conventional Anderson localization. Employing an intuitive optimization approach, we unveiled the universal dynamical scaling in this unconventional non-Hermitian transport, distinctly different from

typical diffusive or ballistic transport. More interestingly, we find a close connection between the scaling behavior and the imaginary-part density of states (iDOS), especially the long-time behavior is dictated by the tail of iDOS. Our findings underscore the fundamental distinction between non-Hermitian and Hermitian localization, particularly in terms of dynamics. Numerous open questions persist, including the theoretical prediction and experimental observation of dynamic behaviors arising from different types of disorders, particularly in the regime with comparable kinetic and potential terms. It is also interesting to explore the combined dynamical consequence of Anderson localization and non-Hermitian skin effect [25–37]. Additionally, the interplay between interactions and non-Hermitian disorders poses an intriguing avenue for exploration. On the experimental front, photonic systems provide a promising platform, as demonstrated by relevant experiments [2]. Furthermore, open systems featuring local random losses, such as dissipative cavity arrays, offer additional opportunities to validate our theory.

Acknowledgements. This work is supported by NSFC under Grant No. 12125405 and National Key R&D Program of China (No. 2023YFA1406702). C.C. acknowledges support from NSFC under Grant No. 12347107.

* wangzhongemail@tsinghua.edu.cn

- [1] P. W. Anderson, ‘‘Absence of diffusion in certain random lattices,’’ *Phys. Rev.* **109**, 1492 (1958).
- [2] S. Weidemann, M. Kremer, S. Longhi, and A. Szameit, ‘‘Coexistence of dynamical delocalization and spectral localization through stochastic dissipation,’’ *Nature Photonics* **15**, 576 (2021).
- [3] S. Longhi, ‘‘Anderson localization in dissipative lattices,’’ *Annalen der Physik* **535**, 2200658 (2023).
- [4] I. I. Yusipov, T. V. Lapyeva, and M. V. Ivanchenko, ‘‘Quantum jumps on anderson attractors,’’ *Phys. Rev. B* **97**, 020301 (2018).
- [5] A. F. Tzortzakakis, K. G. Makris, A. Szameit, and E. N. Economou, ‘‘Transport and spectral features in non-hermitian open systems,’’ *Phys. Rev. Res.* **3**, 013208 (2021).
- [6] A. Leventis, K. G. Makris, and E. N. Economou, ‘‘Non-hermitian jumps in disordered lattices,’’ *Phys. Rev. B* **106**, 064205 (2022).
- [7] H. Sahoo, R. Vijay, and S. Mujumdar, ‘‘Anomalous transport regime in a non-hermitian anderson-localized hybrid system,’’ *Phys. Rev. Res.* **4**, 043081 (2022).
- [8] A. F. Tzortzakakis, K. G. Makris, and E. N. Economou, ‘‘Non-hermitian disorder in two-dimensional optical lattices,’’ *Phys. Rev. B* **101**, 014202 (2020).
- [9] I. Yusipov, T. Lapyeva, S. Denisov, and M. Ivanchenko, ‘‘Localization in open quantum systems,’’ *Phys. Rev. Lett.* **118**, 070402 (2017).
- [10] N. F. Mott, ‘‘Conduction in non-crystalline materials,’’ *The Philosophical Magazine: A Journal of Theoretical Experimental and Applied Physics* **19**, 835 (1969).

- [11] A. Basiri, Y. Bromberg, A. Yamilov, H. Cao, and T. Kotlos, “Light localization induced by a random imaginary refractive index,” *Phys. Rev. A* **90**, 043815 (2014).
- [12] N. Apsley and H. P. Hughes, “Temperature- and field-dependence of hopping conduction in disordered systems,” *The Philosophical Magazine: A Journal of Theoretical Experimental and Applied Physics* **30**, 963 (1974).
- [13] N. Apsley and H. P. Hughes, “Temperature- and field-dependence of hopping conduction in disordered systems, ii,” *The Philosophical Magazine: A Journal of Theoretical Experimental and Applied Physics* **31**, 1327 (1975).
- [14] F. Brochard and P. G. de Gennes, “Dynamics of confined polymer chains,” *The Journal of Chemical Physics* **67**, 52 (1977).
- [15] Y. C. Zhang, “Diffusion in a random potential: Hopping as a dynamical consequence of localization,” *Phys. Rev. Lett.* **56**, 2113 (1986).
- [16] J.-P. Bouchaud and A. Georges, “Anomalous diffusion in disordered media: Statistical mechanisms, models and physical applications,” *Physics Reports* **195**, 127 (1990).
- [17] M. Cates and R. Ball, “Statistics of a polymer in a random potential, with implications for a nonlinear interfacial growth model,” *Journal de Physique* **49**, 2009 (1988).
- [18] T. Halpin-Healy and Y.-C. Zhang, “Kinetic roughening phenomena, stochastic growth, directed polymers and all that. aspects of multidisciplinary statistical mechanics,” *Physics Reports* **254**, 215 (1995).
- [19] According to the extreme statistics theory [38, 39], the expected largest value $\lambda_{|\mathbf{x}|}^{\max}$ in $n = |\mathbf{x}|^d$ trails taken from the cumulative distribution $F^n(\lambda_{|\mathbf{x}|}^{\max}) = \int_{-\infty}^{\lambda_{|\mathbf{x}|}^{\max}} \rho(\lambda) d\lambda = 1 - P_x$ behaves like $F^n(\lambda_{|\mathbf{x}|}^{\max}) \sim 1 - 1/n$, which reproduces $P_x \sim 1/n = |\mathbf{x}|^{-d}$.
- [20] See the Supplementary Materials at [URL will be inserted by publisher] for details of calculation.
- [21] S.-k. Ma and G. F. Mazenko, “Critical dynamics of ferromagnets in $6 - \epsilon$ dimensions: General discussion and detailed calculation,” *Phys. Rev. B* **11**, 4077 (1975).
- [22] D. Forster, D. R. Nelson, and M. J. Stephen, “Large-distance and long-time properties of a randomly stirred fluid,” *Phys. Rev. A* **16**, 732 (1977).
- [23] E. Medina, T. Hwa, M. Kardar, and Y.-C. Zhang, “Burgers equation with correlated noise: Renormalization-group analysis and applications to directed polymers and interface growth,” *Phys. Rev. A* **39**, 3053 (1989).
- [24] T. Nattermann and W. Renz, “Diffusion in a random catalytic environment, polymers in random media, and stochastically growing interfaces,” *Phys. Rev. A* **40**, 4675 (1989).
- [25] S. Yao and Z. Wang, “Edge states and topological invariants of non-hermitian systems,” *Phys. Rev. Lett.* **121**, 086803 (2018).
- [26] F. K. Kunst, E. Edvardsson, J. C. Budich, and E. J. Bergholtz, “Biorthogonal bulk-boundary correspondence in non-hermitian systems,” *Phys. Rev. Lett.* **121**, 026808 (2018).
- [27] L. Xiao, T. Deng, K. Wang, G. Zhu, Z. Wang, W. Yi, and P. Xue, “Non-hermitian bulk-boundary correspondence in quantum dynamics,” *Nature Physics* **16**, 761 (2020).
- [28] T. Helbig, T. Hofmann, S. Imhof, M. Abdelghany, T. Kiessling, L. W. Molenkamp, C. H. Lee, A. Szameit, M. Greiter, and R. Thomale, “Generalized bulk-boundary correspondence in non-hermitian topoelectrical circuits,” *Nature Physics* **16**, 747 (2020).
- [29] V. M. Martinez Alvarez, J. E. Barrios Vargas, and L. E. F. Foa Torres, “Non-hermitian robust edge states in one dimension: Anomalous localization and eigenspace condensation at exceptional points,” *Phys. Rev. B* **97**, 121401 (2018).
- [30] C. H. Lee and R. Thomale, “Anatomy of skin modes and topology in non-hermitian systems,” *Phys. Rev. B* **99**, 201103 (2019).
- [31] Y. Ashida, Z. Gong, and M. Ueda, “Non-hermitian physics,” *Adv. Phys.* **69**, 249 (2020).
- [32] E. J. Bergholtz, J. C. Budich, and F. K. Kunst, “Exceptional topology of non-hermitian systems,” *Rev. Mod. Phys.* **93**, 015005 (2021).
- [33] J. T. Gohsrich, A. Banerjee, and F. K. Kunst, “The non-hermitian skin effect: A perspective,” [arXiv:2410.23845](https://arxiv.org/abs/2410.23845).
- [34] H. Jiang, L.-J. Lang, C. Yang, S.-L. Zhu, and S. Chen, “Interplay of non-hermitian skin effects and anderson localization in nonreciprocal quasiperiodic lattices,” *Phys. Rev. B* **100**, 054301 (2019).
- [35] S. Weidemann, M. Kremer, S. Longhi, and A. Szameit, “Topological triple phase transition in non-hermitian floquet quasicrystals,” *Nature* **601**, 354 (2022).
- [36] Q.-B. Zeng, Y.-B. Yang, and Y. Xu, “Topological phases in non-hermitian aubry-andré-harper models,” *Phys. Rev. B* **101**, 020201 (2020).
- [37] B.-b. Wang, Z. Cheng, H.-y. Zou, Y. Ge, K.-q. Zhao, Q.-r. Si, S.-q. Yuan, H.-x. Sun, H. Xue, and B. Zhang, “Disorder-induced acoustic non-Hermitian skin effect,” [arXiv e-prints](https://arxiv.org/abs/2402.10989), [arXiv:2402.10989](https://arxiv.org/abs/2402.10989) (2024), [arXiv:2402.10989 \[physics.class-ph\]](https://arxiv.org/abs/2402.10989).
- [38] A. Hansen, E. L. Hinrichsen, and S. Roux, “Non-directed polymers in a random medium,” *Journal de Physique I* **3**, 1569 (1993).
- [39] E. Gumbel, *Statistics of Extremes*, Dover Books on Mathematics (Dover Publications, 2012).

Supplemental Material for “Universal non-Hermitian transport in disordered systems”

Bo Li,^{1,2} Chuan Chen,^{3,2} and Zhong Wang^{2,*}

¹*MOE Key Laboratory for Nonequilibrium Synthesis and Modulation of Condensed Matter, Shaanxi Province Key Laboratory of Quantum Information and Quantum Optoelectronic Devices, School of Physics, Xi'an Jiaotong University, Xi'an 710049, China*

²*Institute for Advanced Study, Tsinghua University, Beijing, 100084, China*

³*Lanzhou Center for Theoretical Physics, Key Laboratory of Quantum Theory and Applications of MoE, Key Laboratory of Theoretical Physics of Gansu Province, and School of Physical Science and Technology, Lanzhou University, Lanzhou, Gansu 730000, China*

CONTENTS

I. Dynamical scaling from a Gaussian iDOS	1
II. The imaginary-spectrum density of state (iDOS)	2
A. The strong-disorder limit ($W \gg t_0$)—the linear tail in a bounded disorder	2
B. The weak-disorder limit ($W \ll t_0$)—emergent Gaussian distribution	3
C. Intermediate disorder ($W \sim t_0$)	4
III. Renormalization group analysis	4
IV. In the framework of the Lindblad master equation	8
A. Lattice model with random dissipation	8
B. Purely dissipative lattice model	9
References	10

I. DYNAMICAL SCALING FROM A GAUSSIAN iDOS

Here, we elaborate the replacement-time scaling that arises from a Gaussian iDOS $\rho(\lambda) \sim e^{-\lambda^2/(2\sigma^2)}$. Eq.(2) in the main text is specified as below

$$P_x = \int_{\lambda_x}^{\infty} e^{-\lambda^2} d\lambda \sim |\mathbf{x}|^{-d}. \quad (1)$$

When a large distance is considered, $|\mathbf{x}| \gg 1$, λ_x should be much greater than unity ($t_0 = 1$ is assumed), so that the integral can be estimated by the leading order of expansion around ∞ ,

$$e^{-\lambda_x^2} \frac{1}{\lambda_x} \sim |\mathbf{x}|^{-d}. \quad (2)$$

This leads to

$$\lambda_x \sim \left(d \ln |\mathbf{x}| - \ln \lambda_x + \dots \right)^{1/2}, \quad (3)$$

which generates the leading-order result

$$\lambda_x \sim (d \ln |\mathbf{x}|)^{1/2}. \quad (4)$$

* wangzhongemail@tsinghua.edu.cn

Then, substituting this expression into the optimization equation $\partial W(\mathbf{x}, t)/\partial |\mathbf{x}| = 0$ gives

$$|\mathbf{x}|(\ln |\mathbf{x}|)^{1/2} = \frac{\xi d^{1/2}}{2} t, \quad (5)$$

which further yields

$$\ln |\mathbf{x}| = \ln t - \frac{1}{2} \ln \ln |\mathbf{x}| + \text{const.} = \ln[t/(\ln t)^{1/2}] + \dots \quad (6)$$

where “ \dots ” represents higher-order contributions and a scaling irrelevant constant. In summary, the dominant scaling reads

$$|\mathbf{x}| \sim t/\ln^{1/2} t. \quad (7)$$

Note that the derivation above is only valid for large-distance scaling. Therefore, we anticipate that this relation will fit well with numerical results for $|\mathbf{x}| \gg 1$.

II. THE IMAGINARY-SPECTRUM DENSITY OF STATE (iDOS)

In this section, we study the imaginary-part density of state (iDOS) in the strong and weak disorder limit. In the strong limit for a bounded disorder, the iDOS is dictated by the disorder form, attached with some tails. Here, we focus on the uncorrelated uniform disorder $V \in [-W, W]$ to reveal the origin of the linear tail. Corresponding conclusions for a Gaussian disorder will be commented accordingly. In the weak limit, the emergence of Gaussian-type iDOS is attributed to the central limit theorem and independent of the specific form of disorder. However, when the disorder is comparable with the kinetic term, no simple conclusion can be obtained. Reliable results in this regime might need consulting some advanced random matrix theories, which would be left for future.

A. The strong-disorder limit ($W \gg t_0$)—the linear tail in a bounded disorder

In the case of strong disorder ($W \gg t_0$), the hopping term can be regarded as perturbation to the disorder. In the zero-th order, the local potential value is the eigenvalues. When hopping terms are added, the corrections start from its second order because an off-diagonal perturbation can not contribute in the leading order given that the zero-th order eigenstates are localized strictly. The effect of hopping terms is mixing neighboring (imaginary) potentials to reach some values in between. A naive inference is that, if the magnitude of potential is bounded, the possibility for reaching maximum or minimum imaginary value is less than those moderate values. This is because there are less choices to involve a larger potential than the target value. An extreme case is $V_i = W$, hopping terms can only reduce the magnitude of eigenvalue, thus the possibility of arriving at $\varepsilon = iW$ is zero.

Depending on the magnitude of fluctuations of neighboring potentials, the imaginary part of eigenvalues can be understood under the framework of either normal or degenerate perturbation theory. For simplicity, we take the 1D case as an example, results for higher dimensions can be understood in the same way. For an eigenstate with $\varepsilon_i^{(0)} = iV_i$ (with $V_i \in [-W, W]$), if the local potential of its neighboring sites are not too close, i.e., $|V_{i\pm 1} - V_i| \gg t_0$, the corrected eigenvalue reads (for 1D)

$$\varepsilon_i = iV_i - \frac{it_0^2}{V_i - V_{i+1}} - \frac{it_0^2}{V_i - V_{i-1}} + \dots \quad (8)$$

With sample manipulation under the assumption $|V_{i\pm 1} - V_i| \gg t_0$, it is easy to show the resultant ε_i is bounded by the maximum and minimum value of $\{V_{i-1}, V_i, V_{i+1}\}$. In particular, for $\varepsilon_i^{(0)} = iW$, its imaginary part can be only reduced by corrections from hopping, and, to $O(t_0^2)$, the maximum possible resultant value is

$$\max \text{Im} \varepsilon_i = W - \frac{t_0^2}{W}. \quad (9)$$

For $\lambda \in [W - t_0^2/W, W]$, the growing factor cannot be obtained by the perturbation theory above. Because $t_0^2/W \ll t_0 \ll |V_i - V_{i\pm 1}|$, if the above theory can yield the wanted λ , there must be one or two sites taking potential value far from this range (compare to the width t_0^2/W and t_0) involved to mix with a potential in this range (potentials within this range will not mix by assumption); as a result, the obtained growing factor must be out of this range,

i.e., $\lambda = V_i - t_0^2/(V_i - V_{i+1}) - t_0^2/(V_i - V_{i-1}) < W - t_0^2/W$ with $V_i \in [W - t_0^2/W, W]$ and $V_i > V_{i\pm 1}$ to satisfy the precondition of perturbation formula above.

We are interested the tail density state, i.e., $\rho(\Delta)$ with $\Delta = W - \lambda$ being very small, say less than t_0 . In particular, when $\Delta < t_0^2/W$, the target value can not be reached by Eq. (8); the eigenvalue in this range can only be understood under the framework of the degenerate perturbation theory, namely consider the case $|V_i - V_{i+1}| \lesssim t_0$. This corresponds to the rare events that a small region is fully occupied by potential with similar magnitude [1]. In this region, particles are almost free from disorder, thus hopping terms produce the real part of eigenvalue and the imaginary part is the average of potential in this region. Assuming that the local fluctuation of potential in this region is $\delta < t_0$, and the region size is R^d , then the possibility of such rare event is

$$P \sim \left(\frac{\delta}{2W}\right)^{R^d}, \quad (10)$$

which apparently decreases exponentially as R^d increase. To capture the leading feature of $\rho(\Delta)$, we consider the case with $R = 2$ and $d = 1$ for simplicity, say potential V_1, V_2 on neighboring sites, then degenerate perturbation in the subspace yields

$$\varepsilon = i \frac{V_1 + V_2}{2} \pm \sqrt{t_0^2 - \frac{(V_1 - V_2)^2}{4}}. \quad (11)$$

It is obvious that for a given Δ there is only one freedom of choosing local potential within these two sites; suppose the larger one is counted (the larger one is greater than the target value $\lambda = W - \Delta$), then following relation holds

$$\rho(\Delta) \sim \int_{W-\Delta}^W \frac{d\lambda}{2W} \propto \Delta. \quad (12)$$

If larger R is considered, more freedoms appear and higher orders of Δ will enter the density of state. These contribution will be exponentially suppressed and higher-order terms are overwhelm by the linear term.

For Δ small but greater than t_0^2/W , the main contribution still comes from Eq. (8) (the degenerate-perturbation contribution is exponentially suppressed), so that there are two freedoms (in 1D) of choosing the value of involved local potential and the resultant probability is the joint probability of these two.

$$\begin{aligned} \rho(\lambda) &\sim \int_{\lambda}^W d\lambda_1 P(V_{\max} = \lambda_1) \int d\lambda_2 P(\text{one of the rest value} = \lambda_2 | V_{\max} = \lambda_1) \\ &= \int_{\lambda}^W \frac{d\lambda_1}{2W} \int_{-W}^{B(\lambda_1, \lambda)} \frac{d\lambda_2}{2W} \\ &= \frac{W(W - \lambda)}{(2W)^2} + \frac{1}{(2W)^2} \int d\lambda_1 B(\lambda_1, \lambda) \\ &\sim \Delta + \mathcal{O}(\Delta^2) \end{aligned} \quad (13)$$

where $\lambda = W - \Delta \sim W$. Here, it is not hard to show that the lower bound of λ_2 is $-W$, and the upper bound is a function of λ and λ_1 . The coefficient in front of Δ in the last line is not explicitly given because the second term in the second line from bottom could also produce a linear term. In particular, the higher-order terms are highly suppressed near the band edge, thus a linear behavior for $\rho(\lambda)$ is seen near the edge if the imaginary part of spectrum is bounded.

B. The weak-disorder limit ($W \ll t_0$)—emergent Gaussian distribution

In a weak disorder, the localization length is large, so that the eigenstates cover many sites with number $\sim \xi^d$, where ξ is generally a function of eigenvalue ε and mainly relies on $\text{Re}(\varepsilon)$ for weak non-Hermitian disorder. This picture is especially valid for these states in the middle of real part of band, i.e., $\text{Re}(\varepsilon) \approx 0$. The corresponding imaginary part of energy is asymptotically given by the average of local potential in these sites, which respects a Gaussian distribution, according to central limit theorem. This can be seen more explicitly from a perturbative perspective. In 1D, near the band center, the unperturbed wave function is $\psi_j^{(0)} \sim e^{ikj}$ with $k \simeq \pm\pi/2$, and with imaginary disorder counted in the eigenstate is given by a linear combination of states in a narrow region near k , i.e.,

$$\psi^R \approx \sum_{q \in [k-\epsilon, k+\epsilon]} c_q \psi_q^{(0)}, \quad \epsilon \sim W/t_0 \ll 1. \quad (14)$$

Here, the narrow region works much better around the band center than the band edge. From perturbation theory, the linear combination should include all bands within a range W/t_0 . For $k = \pm\pi/2 + \epsilon$, $\delta E(k) = E(\pm\pi/2 + \epsilon) - E(\pm\pi/2) \sim t_0\epsilon \sim W$, so $\epsilon \sim W/t_0$; however, around the band edge ($k = 0$ or π), $\delta E = E(\epsilon) - E(0) \sim t_0\epsilon^2 \sim W$, which yields $\epsilon \sim (W/t_0)^{1/2}$. For $W/t_0 \ll 1$, the state near the band edge needs to involve much more states. Turning to real space, this means the states near the band center has a longer localization length, while that near the edge usually are sharper because of that the reciprocal space components for a narrow peak should take broader distribution, e.g., the Dirac-delta function is superposition of plane wave with all momentum components.

The property $H^\dagger = H^*$ enforces $\langle \psi^L | = (|\psi^R\rangle)^T$, thus the normalization relation is given by

$$\langle \psi^L | \psi^R \rangle = \sum_j \sum_{q,q'} c_q c_{q'} \psi_{q,j}^{(0)} \psi_{q',j}^{(0)} = \sum_q c_q^2 = 1. \quad (15)$$

Taking disorder into account, the eigenvalues is

$$\varepsilon = \varepsilon_1 + \varepsilon_2 = \langle \psi^L | H_0 | \psi^R \rangle + i \langle \psi^L | V | \psi^R \rangle. \quad (16)$$

Here,

$$\varepsilon_1 = \sum_q c_q^2 \varepsilon_q^{(0)} \simeq \varepsilon_k^{(0)} \sum_q c_q^2 = \varepsilon_k^{(0)} \quad (17)$$

which is real, and the second part

$$\varepsilon_2 = i \sum_j |\psi_j^R|^2 V_j \simeq i (\sum_j V_j) / \xi, \quad (18)$$

which respects Gaussian distribution by the central limit theorem. Here, the approximation $|\psi_j^R|^2 \simeq 1/\xi$ is used, which is better justified for small q , i.e., near the band center. In summary, the growing factor obeys the following distribution

$$P(\lambda = \text{Im}\varepsilon_2) \propto e^{-\lambda^2/(2\sigma_\lambda^2)} \quad (19)$$

where

$$\sigma_\lambda \simeq \frac{\sigma_V}{\sqrt{\xi}} \sim \frac{W}{\sqrt{\xi}}. \quad (20)$$

Here, $\sigma_V = \sqrt{\langle V^2 \rangle} = W/\sqrt{3}$. Note the analysis above gradually fails when for k deviate from $\pm\pi/2$ as the relation $|\psi_j^R|^2 = 1/\xi$ becomes invalid as approaching the (real part of) band edge. In other words, the Gaussian distribution fits well for eigenvalues with its eigenstates having a long wavelength, which can meet the condition for central limit theorem better.

C. Intermediate disorder ($W \sim t_0$)

In the presence of an intermediate disorder with $W \sim t_0$, the form of iDOS can not be easily identified. However, it is expected that the iDOS would bridge the two extreme cases with strong or weak disorders, such that the long-time scaling in this scenario exhibits a crossover behavior. Indeed, via numerical simulation in Fig. 1, we find the scaling falls in between the scaling forms dominated by the Gaussian (weak-disorder limit) and the linear (strong-disorder limit) iDOS.

III. RENORMALIZATION GROUP ANALYSIS

In this section, we follow Ref. [2] to carry out a dynamical renormalization group analysis. In the long-wavelength limit, the system is governed by a Schrödinger equation

$$i\partial_t \psi(\mathbf{x}, t) = [-D\nabla^2 + iV(\mathbf{x})]\psi(\mathbf{x}, t) \quad (21)$$

where $D = \eta = t_0$ (set $\hbar = 1$), and

$$\langle V(\mathbf{x})V(\mathbf{x}') \rangle = v\delta^d(\mathbf{x} - \mathbf{x}') \quad (22)$$

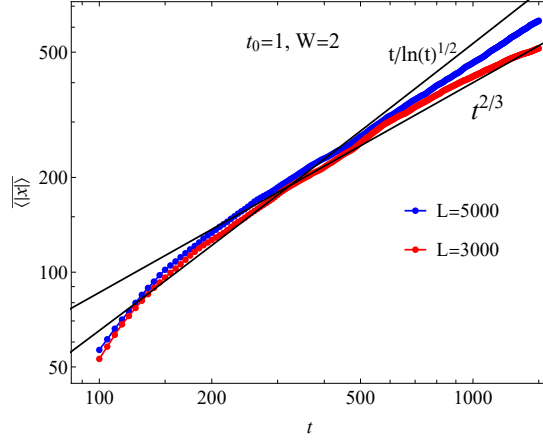


FIG. 1. Scaling for intermediate disorder with $W = 2t_0$, where 500 realizations of disorder are performed.

with v reflecting the disorder strength. Performing a Cole-Hopf transformation $\psi(\mathbf{x}, t) = \exp(\Phi(\mathbf{x}, t))$, the Schrodinger equation is converted to

$$\partial_t \Phi = iD\nabla^2 \Phi + i\eta(\nabla \Phi)^2 + V(\mathbf{x}). \quad (23)$$

Turning to the momentum-frequency space via Fourier and Laplace transformation

$$\Phi(\mathbf{x}, t) = \int_{\gamma-i\infty}^{\gamma+i\infty} \frac{ds}{2\pi i} \int_{k<\Lambda} \frac{d^d k}{(2\pi)^d} e^{i\mathbf{k}\cdot\mathbf{x}+st} \Phi(\mathbf{k}, s) \quad (24)$$

where $\gamma \in \mathbb{R}$ is chosen to make the integral kernel convergent, i.e., all singularities lying at the left of line $z = \gamma$ on the complex plane, and

$$V(\mathbf{k}, s) = i2\pi\delta(s)V(\mathbf{k}), \quad \text{with} \quad \langle V(\mathbf{k})V(\mathbf{k}') \rangle = v(2\pi)^d \delta^d(\mathbf{k} + \mathbf{k}'). \quad (25)$$

Here, the Laplace transformation is applied in consideration of the complex eigenvalues in our system. Substituting Eq. (24) into Eq. (23) results in

$$\Phi(\mathbf{k}, s) = G_0(\mathbf{k}, s)V(\mathbf{k}, s) - i\eta G_0(\mathbf{k}, s) \int_{\Omega, \mathbf{q}} \mathbf{q} \cdot (\mathbf{k} - \mathbf{q}) \Phi(\mathbf{q}, \Omega) \Phi(\mathbf{k} - \mathbf{q}, s - \Omega) \quad (26)$$

where $\int_{\Omega, \mathbf{q}} = \int_{\gamma-i\infty}^{\gamma+i\infty} d\Omega / (i2\pi) \int d^d q / (2\pi)^d$ and

$$G_0(\mathbf{k}, s) = \frac{1}{s + iDk^2}. \quad (27)$$

The one-loop correction to Green function is shown diagrammatically in Fig. 2, which is written as

$$G(\mathbf{k}, s) = G_0(\mathbf{k}, s) + 4(-i\eta)^2 G_0(\mathbf{k}, s) \int_{\mathbf{q}, \Omega} \left[\left(\frac{\mathbf{k}}{2} - \mathbf{q} \right) \cdot \left(\frac{\mathbf{k}}{2} + \mathbf{q} \right) \right] \left[\mathbf{k} \cdot \left(-\frac{\mathbf{k}}{2} + \mathbf{q} \right) \right] G_0\left(\frac{\mathbf{k}}{2} + \mathbf{q}, \frac{s}{2} + \Omega \right) C\left(\frac{\mathbf{k}}{2} - \mathbf{q}, \frac{s}{2} - \Omega \right), \quad (28)$$

and

$$C(\mathbf{q}, \Omega) = \int_{\mathbf{k}, \omega} \langle \Phi_0(\mathbf{q}, \Omega) \Phi_0(\mathbf{k}, \omega) \rangle = i2\pi v G_0(\mathbf{q}, \Omega) G_0(-\mathbf{q}, -\Omega) \delta(\Omega), \quad (29)$$

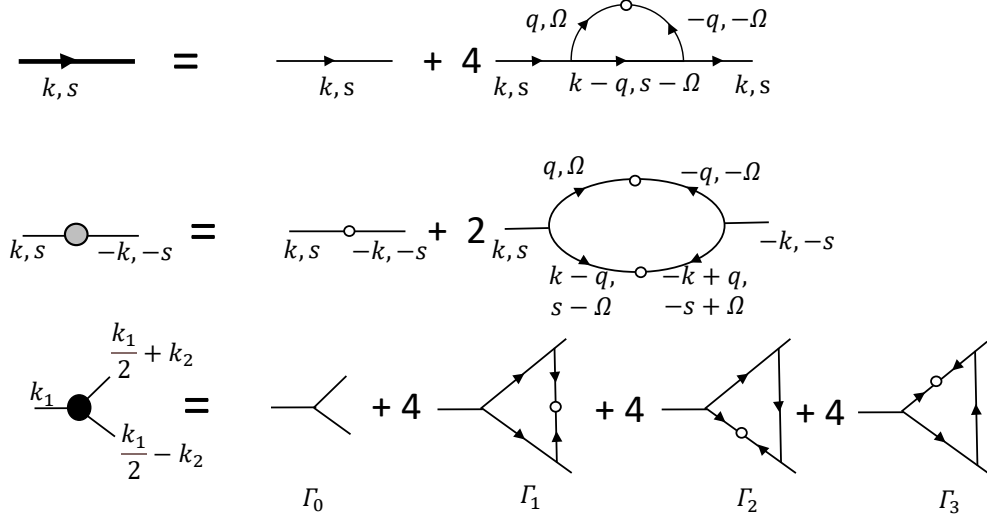


FIG. 2. By averaging over disorders, the corresponding functions will be renormalized. In the diagrams above, corrections up to the third order of η are considered. The diagrams respectively describe renormalized (Top) Green function, (Middle) correlator, and (Bottom) vertex. The thin and thick line represent the bare and renormalized Green function, respectively; the thin line with a small open circle donates the bare correlator, while the thin line with a gray solid disk stands for the renormalized correlator; the black solid disk is the renormalized vertex.

with $\Phi_0(\mathbf{q}, \Omega) = G_0(\mathbf{q}, \Omega)V(\mathbf{q}, \Omega)$. Then second term in the limit $\mathbf{k} \rightarrow 0$ and $s \rightarrow 0$ is given as

$$\begin{aligned}
I(\mathbf{k}, s) &= \frac{-4v\eta^2 G_0^2(\mathbf{k}, s)}{(2\pi)^d} \int_{\gamma-i\infty}^{\gamma+i\infty} d\Omega \int d^d q \left(\frac{k^2}{4} - q^2 \right) \left(-\frac{k^2}{2} + kq \cos \theta \right) \frac{1}{\frac{s}{2} + \Omega + iD|\frac{\mathbf{k}}{2} + \mathbf{q}|^2} \\
&\times \frac{1}{\frac{s}{2} - \Omega + iD|\frac{\mathbf{k}}{2} - \mathbf{q}|^2} \frac{1}{-\frac{s}{2} + \Omega + iD|\frac{\mathbf{k}}{2} + \mathbf{q}|^2} \delta\left(\frac{s}{2} - \Omega\right) \\
&= \frac{-4v\eta^2}{(2\pi)^d} \frac{1}{(iDk^2)^2} \int d^d q \frac{\left(\frac{k^2}{4} - q^2\right) \left(-\frac{k^2}{2} + kq \cos \theta\right)}{(iD)^3 \left(\frac{k^2}{2} + q^2 + kq \cos \theta\right) \left(\frac{k^2}{2} + q^2 + kq \cos \theta\right)^2} \\
&= \frac{-4v\eta^2}{i(2\pi)^d} \frac{1}{D^5 k^4} \int dq q^{d-1} S_{d-1} \int_0^\pi d\theta \sin^{(d-2)} \theta [q^{-4} k^2 \left(\frac{1}{2} - \cos^2 \theta\right) + \text{higher orders of } k] \\
&= \frac{-v\eta^2 K_d}{iD^5} \frac{2(d-2)}{d} \frac{1}{k^2} \int dq q^{d-5}
\end{aligned} \tag{30}$$

where we used $S_{d-1} \int_0^\pi d\theta \sin^{(d-2)} \theta \cos^2 \theta = (S_{d-1}/d) \int_0^\pi \sin^{(d-2)} \theta = S_d/d$, and $K_d = S_d/(2\pi)^d$. By the results above, we obtain the renormalized parameter \tilde{D} is given by

$$\tilde{D} = D \left(1 + \frac{2(d-2)v\eta^2 K_d}{dD^4} \int dq q^{d-5} \right). \tag{31}$$

The one-loop correction to correlator $C(\mathbf{k}, s)$ is given by the second line in Fig. 2, which further gives the correction to the disorder strength in the limit $\mathbf{k} \rightarrow 0$ and $s \rightarrow 0$ as below

$$\begin{aligned}
\tilde{v} &= v + \lim_{\mathbf{k} \rightarrow 0, s \rightarrow 0} \frac{2}{i(2\pi)} (-i\eta)^2 \int_{\mathbf{q}, \Omega} [(\mathbf{k} - \mathbf{q}) \cdot \mathbf{q}]^2 C(\mathbf{q}, \Omega) C(\mathbf{k} - \mathbf{q}, s - \Omega) \\
&= v + 2(-i\eta)^2 v^2 (i2\pi) \frac{S_d}{i(2\pi)^{d+1}} \int dq q^{d-1} q^4 G_0(\mathbf{q}, 0) G_0(-\mathbf{q}, 0) G_0(-\mathbf{q}, 0) G_0(\mathbf{q}, 0) \\
&= v - \frac{2v^2 \eta^2}{D^4} K_d \int dq q^{d-5}.
\end{aligned} \tag{32}$$

Here, the $i2\pi$ in the first line is put there to cancel extra $i2\pi$ in $C(\dots)$ functions because it can be shown that to

form one loop by averaging disorder, there only has one $i2\pi$ factor left even if higher order correlator, e.g. $\langle VVVV \rangle$, are evolved in, other factors cancel with vertex integral (generating $C(\mathbf{q}, \Omega)$) to close the loop.

The third line gives corrections to η as

$$\tilde{\eta} = \eta(1 + \gamma_1 + \gamma_2 + \gamma_3), \quad (33)$$

with γ_i corresponding the correction from Γ_i ($i = 1, 2, 3$). Specifically,

$$\begin{aligned} \gamma_1 &= \lim_{\mathbf{k}_{1,2} \rightarrow 0} \lim_{s_{1,2} \rightarrow 0} \frac{\Gamma_1}{\Gamma_0} \\ &= \lim_{\mathbf{k}_{1,2} \rightarrow 0} \lim_{s_{1,2} \rightarrow 0} \frac{4(-i\eta)^3}{-i\eta(\frac{\mathbf{k}_1}{2} + \mathbf{k}_2) \cdot (\frac{\mathbf{k}_1}{2} - \mathbf{k}_2)} \int_{\mathbf{q}, \Omega} U_1(\mathbf{k}_1, \mathbf{k}_2, \mathbf{q}) G_0(\frac{\mathbf{k}_1}{2} + \mathbf{q}, \frac{s_1}{2} + \Omega) G_0(\frac{\mathbf{k}_1}{2} - \mathbf{q}, \frac{s_1}{2} - \Omega) C(\mathbf{q} - \mathbf{k}_1, \Omega - s_2) \\ &= 4(-i\eta)^2 v \int \frac{d^d q}{(2\pi)^d} \frac{1}{(iDq^2)^4} \frac{q^4(\frac{k_1^2}{2} \cos^2 \theta_1 - k_2^2 \cos^2 \theta_2)}{\frac{k_1^2}{4} - k_2^2} \\ &= -\frac{4\eta^2 v}{dD^4} K_d \int dq q^{d-5}. \end{aligned} \quad (34)$$

Here, we used

$$\begin{aligned} U_1(\mathbf{k}_1, \mathbf{k}_2, \mathbf{q}) &= \left[\left(\frac{\mathbf{k}_1}{2} + \mathbf{q} \right) \cdot \left(\frac{\mathbf{k}_1}{2} - \mathbf{q} \right) \right] \left[\left(\frac{\mathbf{k}_1}{2} - \mathbf{k}_2 \right) \cdot (\mathbf{k}_2 - \mathbf{q}) \right] \left[\left(\frac{\mathbf{k}_1}{2} + \mathbf{k}_2 \right) \cdot (\mathbf{q} - \mathbf{k}_2) \right] \\ &= -q^2 \left(\mathbf{k}_2 - \frac{\mathbf{k}_1}{2} \right) \cdot \mathbf{q} \left(\mathbf{k}_2 + \frac{\mathbf{k}_1}{2} \right) \cdot \mathbf{q} + (\text{higher orders of } k_{1,2}). \end{aligned} \quad (35)$$

In a similar way, we can obtain the other two vertex corrections

$$\begin{aligned} \gamma_3 = \gamma_2 &= \lim_{\mathbf{k}_{1,2} \rightarrow 0} \lim_{s_{1,2} \rightarrow 0} \frac{\Gamma_2}{\Gamma_0} \\ &= \lim_{\mathbf{k}_{1,2} \rightarrow 0} \lim_{s_{1,2} \rightarrow 0} \frac{4(-i\eta)^3}{-i\eta(\frac{\mathbf{k}_1}{2} + \mathbf{k}_2) \cdot (\frac{\mathbf{k}_1}{2} - \mathbf{k}_2)} \int_{\mathbf{q}, \Omega} U_2(\mathbf{k}_1, \mathbf{k}_2, \mathbf{q}) G_0(\frac{\mathbf{k}_1}{2} + \mathbf{q}, \frac{s_1}{2} + \Omega) G_0(\mathbf{q} - \mathbf{k}_2) C(\frac{\mathbf{k}_1}{2} - \mathbf{q}) \\ &= \frac{4\eta^2 v}{dD^4} K_d \int dq q^{d-5} = -\gamma_1 \end{aligned} \quad (36)$$

where we omitted the frequency argument in the expression, and used

$$\begin{aligned} U_2(\mathbf{k}_1, \mathbf{k}_2, \mathbf{q}) &= \left[\left(\frac{\mathbf{k}_1}{2} + \mathbf{q} \right) \cdot \left(\frac{\mathbf{k}_1}{2} - \mathbf{q} \right) \right] \left[\left(\frac{\mathbf{k}_1}{2} + \mathbf{k}_2 \right) \cdot (\mathbf{q} - \mathbf{k}_2) \right] \left[\left(\mathbf{q} - \frac{\mathbf{k}_1}{2} \right) \cdot \left(\frac{\mathbf{k}_1}{2} - \mathbf{k}_2 \right) \right] \\ &= q^2 \left(\mathbf{k}_2 - \frac{\mathbf{k}_1}{2} \right) \cdot \mathbf{q} \left(\mathbf{k}_2 + \frac{\mathbf{k}_1}{2} \right) \cdot \mathbf{q} + (\text{higher orders of } k_{1,2}). \end{aligned} \quad (37)$$

Summarizing three terms up, we obtain the dressed vertex is given by

$$\tilde{\eta} = \eta \left(1 + \frac{4\eta^2 v}{dD^4} K_d \int dq q^{d-5} \right). \quad (38)$$

It is obvious that all integrals induced by corrections is divergent for $d < 4$. This difficulty can be resolved by performing a renormalization group (RG) analysis. Take the integral over a small shell $q \in [e^l, 1]$ (setting $\Lambda = 1$ for convenience) to obtain

$$\begin{aligned} \tilde{D} &= D \left[1 + \frac{2(d-2)v\eta^2 K_d}{dD^4} \frac{1 - e^{(4-d)l}}{(d-4)} \right], \\ \tilde{v} &= v \left[1 - \frac{2v\eta^2}{D^4} K_d \frac{1 - e^{(4-d)l}}{(d-4)} \right], \\ \tilde{\eta} &= \eta \left[1 + \frac{4v\eta^2 K_d}{dD^4} \frac{1 - e^{(4-d)l}}{(d-4)} \right]. \end{aligned} \quad (39)$$

Now, we rescale the variables to compensate the integral over the momentum shell, $\mathbf{x} \rightarrow e^l \mathbf{x}$, $t \rightarrow e^{z l} t$, and $\Phi \rightarrow e^{\chi l} \Phi$. The the modified dynamic equation becomes

$$\partial_t \Phi = i e^{(z-2)l} \tilde{D} \nabla^2 \Phi + i e^{(\chi+z-2)l} \tilde{\eta} (\nabla \Phi)^2 + e^{(z-\chi)l} \tilde{V}(e^l \mathbf{x}). \quad (40)$$

By identifying the modified coefficient as a function of l and take $l = \delta l \ll 1$, we can obtain the following differential recursion relations

$$\begin{aligned} \frac{dD}{dl} &= D(z - 2 + \frac{2(d-2)v\eta^2 K_d}{dD^4}), \\ \frac{dv}{dl} &= v[2(z - \chi - \frac{d}{2}) - \frac{2v\eta^2}{D^4} K_d], \\ \frac{d\eta}{dl} &= \eta(\chi + z - 2 + \frac{4v\eta^2 K_d}{dD^4}). \end{aligned} \quad (41)$$

The RG equations above can yield the differential equation for a coupling constant $g = v\eta^2/D^4$,

$$\frac{dg}{dl} = g[4 - d + \frac{2(12-5d)}{d} K_d g]. \quad (42)$$

There are two fixed points, $g_1^* = 0$, $g_2^* = d(d-4)/[2(12-5d)K_d]$. It is easy to obtain that for $g_1 = g_1^* + \delta g_1$

$$\frac{d\delta g_1}{dl} = (4-d)\delta g_1 + \dots, \quad (43)$$

which implies that g_1^* is unstable for $d < 4$. For $d < 12/5$, $g_2^* < 0$, which is unphysical because g is positive by definition. However, for $d = 3$, $g_2^* = 1/(2K_d)$ is indeed a fixed point. At this fixed point, followed from Eq. (41), we obtain

$$z = 5/3, \quad \chi = 2/3. \quad (44)$$

Since $\chi < 1$, this fixed point is stable against higher-order terms of $i\eta(\nabla\Phi)^2$ generated from RG process associated with Eq. (23).

IV. IN THE FRAMEWORK OF THE LINDBLAD MASTER EQUATION

We consider general open systems with random losses described by the Lindblad master equation. It can be shown that the dynamics respects the same scaling theory outlined in the main text.

A. Lattice model with random dissipation

We consider an open system described by the following master equation of density matrix $\hat{\rho}$

$$\frac{d\hat{\rho}}{dt} = -i[\hat{H}_0, \hat{\rho}] + \sum_{\mathbf{x}} \gamma_{\mathbf{x}} \mathcal{D}[\hat{a}_{\mathbf{x}}] \hat{\rho} \quad (45)$$

where $\hat{H}_0 = \sum_{\mathbf{x}, \mathbf{x}'} h_{\mathbf{x}, \mathbf{x}'} \hat{a}_{\mathbf{x}}^\dagger \hat{a}_{\mathbf{x}'}$ with \mathbf{x}, \mathbf{x}' labeling lattice sites, and $\mathcal{D}[\hat{O}] \hat{\rho} = \hat{O} \hat{\rho} \hat{O}^\dagger - \frac{1}{2}(\hat{O}^\dagger \hat{O} \hat{\rho} + \hat{\rho} \hat{O}^\dagger \hat{O})$ with $\hat{O} = \hat{a}_{\mathbf{x}}$. On the r.h.s. of Eq. (45), the first term describes an unitary evolution given by a Hermitian Hamiltonian \hat{H}_0 , and the second term donates to local losses with site-dependent random rate $\gamma_{\mathbf{x}}$. For a time-independent operator \hat{A} , its averaged value respects the following equation

$$\begin{aligned} \frac{d\langle \hat{A} \rangle}{dt} &= -i \text{Tr}([\hat{H}_0, \hat{\rho}] \hat{A}) + \sum_{\mathbf{x}} \gamma_{\mathbf{x}} \text{Tr}(\mathcal{D}[\hat{a}_{\mathbf{x}}] \hat{\rho} \hat{A}) \\ &= -i \text{Tr}(\hat{\rho} [\hat{A}, \hat{H}_0]) + \frac{1}{2} \sum_{\mathbf{x}} \gamma_{\mathbf{x}} \text{Tr}(\hat{\rho} \hat{a}_{\mathbf{x}}^\dagger [\hat{A}, \hat{a}_{\mathbf{x}}] + \hat{\rho} [\hat{a}_{\mathbf{x}}^\dagger, \hat{A}] \hat{a}_{\mathbf{x}}). \end{aligned} \quad (46)$$

For our purpose, we consider a bilinear operator $\hat{A} = \hat{a}_{\mathbf{x}_1}^\dagger \hat{a}_{\mathbf{x}_2}$ whose average gives the two-point correlation function $G_{\mathbf{x}_1, \mathbf{x}_2} = \langle \hat{a}_{\mathbf{x}_1}^\dagger \hat{a}_{\mathbf{x}_2} \rangle = \text{Tr}[\hat{\rho}(\hat{a}_{\mathbf{x}_1}^\dagger \hat{a}_{\mathbf{x}_2})]$. Through a straightforward calculation, we obtain the dynamic equation of the correlation function

$$\frac{dG_{\mathbf{x}_1, \mathbf{x}_2}}{dt} = i \sum_{\mathbf{x}'} (h_{\mathbf{x}_1, \mathbf{x}'}^T G_{\mathbf{x}', \mathbf{x}_2} - G_{\mathbf{x}_1, \mathbf{x}'} h_{\mathbf{x}', \mathbf{x}_2}^T) - \frac{\gamma_{\mathbf{x}_1} + \gamma_{\mathbf{x}_2}}{2} G_{\mathbf{x}_1, \mathbf{x}_2}. \quad (47)$$

This equation can be reduced to the dynamical equation of correlation matrix $G = G_{\mathbf{x}_1, \mathbf{x}_2} |\mathbf{x}_1\rangle \langle \mathbf{x}_2|$ as below

$$\frac{dG}{dt} = i[(h^T + iV)G - G(h^T - iV)] = i(HG - GH^\dagger) \quad (48)$$

where $H = h^T + iV$ describes a Hermitian system h^T in a random imaginary disorder iV , and V is a diagonal matrix with $V_{\mathbf{x}, \mathbf{x}'} = \gamma_{\mathbf{x}} \delta_{\mathbf{x}, \mathbf{x}'}$. The general solution of the correlation matrix is

$$G(t) = e^{iHt} G(0) e^{-iH^\dagger t}. \quad (49)$$

We are interested in the case that N bosonic particles initially locate at at $\mathbf{x} = \mathbf{0}$, i.e., $G(0) = N|\mathbf{0}\rangle \langle \mathbf{0}|$, the correlation at time t becomes

$$G(t) = N|\psi(t)\rangle \langle \psi(t)| \quad (50)$$

with $|\psi(t)\rangle = e^{iHt} |\mathbf{0}\rangle$. Correspondingly, the particle spreading distance for survived particles in the system is evaluated as

$$\langle |\mathbf{x}| \rangle = \sum_{\mathbf{x}} |\mathbf{x}| G_{\mathbf{x}, \mathbf{x}'}(t) / \sum_{\mathbf{x}} G_{\mathbf{x}, \mathbf{x}'}(t) = \sum_{\mathbf{x}} |\mathbf{x}| |\langle \mathbf{x} | \psi(t) \rangle|^2 / \sum_{\mathbf{x}} |\langle \mathbf{x} | \psi(t) \rangle|^2. \quad (51)$$

Since $|\psi(t)\rangle$ evolves by following the ‘‘Hamiltonian’’ H , it can be also projected into the eigenbasis of H . Considering that H describes a Hermitian Hamiltonian perturbed by a imaginary disorder, the calculation of spreading distance is exactly mapped to the scenario we discussed before.

B. Purely dissipative lattice model

It has been shown that the discrete jumpy motion also appears in a 1D purely dissipative lattice model in Ref. [3]. Here, we generalize this model to higher dimensions and show that the corresponding dynamics can be also characterized by the scaling theory outlined in the main text.

We consider a d -dimensional purely dissipative lattice model whose dynamics is governed by the master equation of density matrix $\hat{\rho}$

$$\frac{d\hat{\rho}}{dt} = \sum_{\mathbf{x}} \Gamma \mathcal{D}[\hat{z}_{\mathbf{x}}] \hat{\rho} + \gamma_{\mathbf{x}} \mathcal{D}[\hat{a}_{\mathbf{x}}] \hat{\rho} \quad (52)$$

where $\hat{z}_{\mathbf{x}} = \hat{a}_{\mathbf{x}} + \sum_{\boldsymbol{\delta}} \hat{a}_{\mathbf{x}+\boldsymbol{\delta}}$ with $\boldsymbol{\delta}$ being the unit vector in a d -dimensional lattice model. The two terms on the r.h.s. of Eq. (52) describe dissipative couplings between adjacent sites with a rate Γ , and local losses with site-dependent random rate $\gamma_{\mathbf{x}}$, respectively. In this model, the unitary evolution part does not appear in the master equation due to the absence of Hermitian Hamiltonian. Similar as before, the dynamics of two-point correlation function $G_{\mathbf{x}_1, \mathbf{x}_2} = \langle \hat{a}_{\mathbf{x}_1}^\dagger \hat{a}_{\mathbf{x}_2} \rangle$ can be obtained by a straightforward calculation

$$\begin{aligned} \frac{dG_{\mathbf{x}_1, \mathbf{x}_2}}{dt} &= -(2\Gamma + \frac{\gamma_{\mathbf{x}_1} + \gamma_{\mathbf{x}_2}}{2}) G_{\mathbf{x}_1, \mathbf{x}_2} - \frac{\Gamma}{2} \sum_{\boldsymbol{\delta}} (G_{\mathbf{x}_1+\boldsymbol{\delta}, \mathbf{x}_2} + G_{\mathbf{x}_1-\boldsymbol{\delta}, \mathbf{x}_2} + G_{\mathbf{x}_1, \mathbf{x}_2+\boldsymbol{\delta}} + G_{\mathbf{x}_1, \mathbf{x}_2-\boldsymbol{\delta}}) \\ &\quad - \frac{\Gamma}{2} \sum_{\boldsymbol{\delta} \neq \boldsymbol{\delta}'} (G_{\mathbf{x}_1+\boldsymbol{\delta}-\boldsymbol{\delta}', \mathbf{x}_2} + G_{\mathbf{x}_1, \mathbf{x}_2+\boldsymbol{\delta}-\boldsymbol{\delta}'}). \end{aligned} \quad (53)$$

This equation can be packed into a matrix form as below

$$\frac{dG}{dt} = HG + GH \quad (54)$$

where

$$H = - \sum_{\mathbf{x}} \left(\Gamma + \frac{\gamma_{\mathbf{x}}}{2} \right) |\mathbf{x}\rangle\langle\mathbf{x}| - \sum_{\mathbf{x}} \sum_{\delta} \frac{\Gamma}{2} (|\mathbf{x}\rangle\langle\mathbf{x} + \delta| + |\mathbf{x}\rangle\langle\mathbf{x} - \delta|) - \sum_{\mathbf{x}} \sum_{\delta \neq \delta'} \frac{\Gamma}{2} |\mathbf{x}\rangle\langle\mathbf{x} + \delta - \delta'|. \quad (55)$$

Here, H describes a Hermitian Anderson model with strictly negative eigenvalues given that $\Gamma, \gamma_{\mathbf{x}} > 0$. Directly solving the correlation function yields $G(t) = e^{Ht}G(0)G^{Ht}$. Following the previous logic, the spreading distance is governed by a “state” of form $|\psi(t)\rangle = e^{Ht}|\mathbf{0}\rangle$ for particles initially sitting at $\mathbf{x} = \mathbf{0}$. Since here the dissipative evolution (reflected as an imaginary time) is dictated by a Hermitian H , the corresponding scaling behavior will be dominated by the density of state (DOS) of H , instead of iDOS. Otherwise, the analysis is analogous to the non-Hermitian case.

-
- [1] P. G. Silvestrov, Phys. Rev. B **64**, 075114 (2001), URL <https://link.aps.org/doi/10.1103/PhysRevB.64.075114>.
 [2] E. Medina, T. Hwa, M. Kardar, and Y.-C. Zhang, Phys. Rev. A **39**, 3053 (1989), URL <https://link.aps.org/doi/10.1103/PhysRevA.39.3053>.
 [3] S. Longhi, Annalen der Physik **535**, 2200658 (2023).